Electronic Supplementary Material (ESI) for Journal of Materials Chemistry A.

Supporting Information

Low-Temperature, High-Performance Thin-Film Solid Oxide Fuel Cells with Tailored Nano-Column Structures of a Sputtered Ni Anode

Wonjong Yu, Yonghyun Lim, Sanghoon Lee, Arunkumar Pandiyan, Gu Young Cho, and Suk Won Cha**

1. STEM-EDX analysis of TF-SOFCs

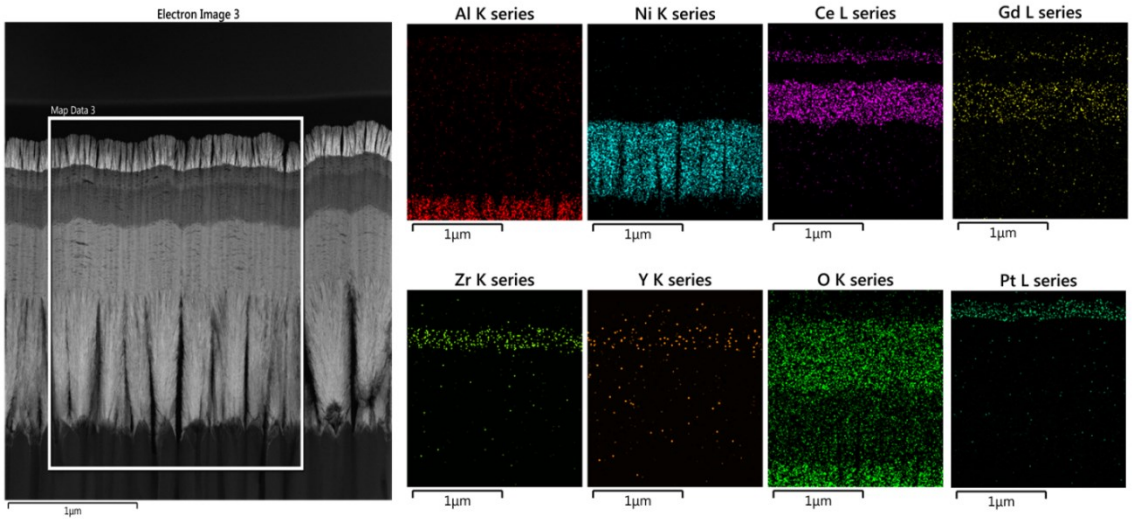

Fig. S1. STEM-EDX images of TF-SOFCs. The distribution of elements is analyzed by mapping the white line box region.

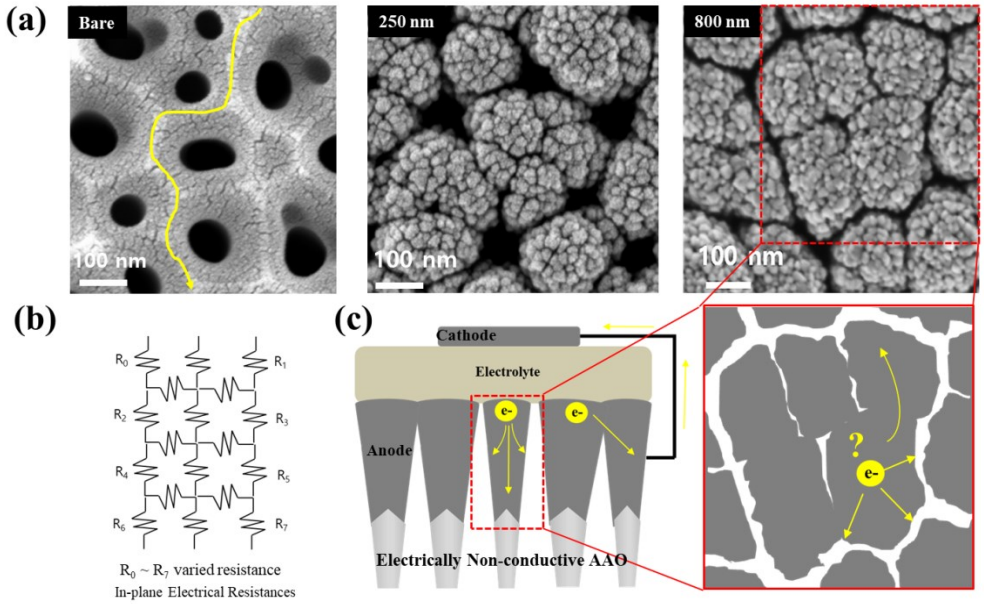

Fig. S2. (a) Surface FESEM views of bare AAO substrate, 250nm-thick, and 800nm-thick sputtered anodes. (b) Conceptual equivalent-circuit for current collecting in sputtered Ni anode deposited on nanoporous AAO substrate. (c) A schematic illustration of an electron pathway produced from the electrolyte/electrode interface in AAO supported TF-SOFCs architecture.

2. XRD analysis for the sputtered anodes.

Table S1. Texture coefficient (TC) calculated for the sputtered Ni anodes on amorphous quartz wafer.

Sample Detail	***(111)***	***(200)***	***(220)***
ROT1(45°)	1.38	0.78	0.82
ROT3(45°)	1.45	0.97	0.55
ROT2(45°)	1.46	0.76	0.76
ROT1(75°)	1.48	0.88	0.63

3. Electrochemical performance of TF-SOFCs with nanostructured Ni anode.

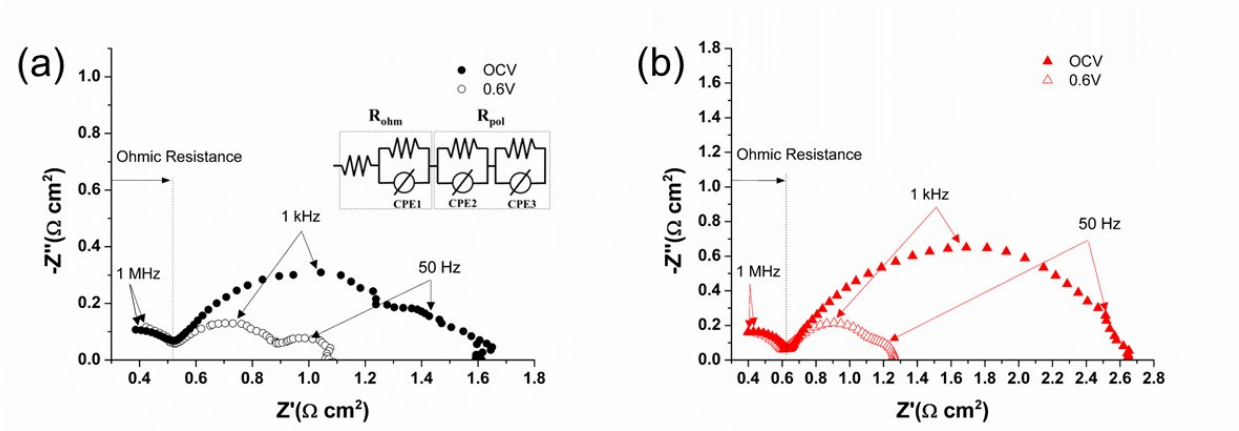

Fig. S3. Electrochemical impedance spectroscopy (EIS) analysis of (a) ROT1(75°) and (b) ROT1(45°) cells measured at 0.6 and OCV.

5. Performance comparison of low temperature solid oxide fuels (LT-SOFCs)

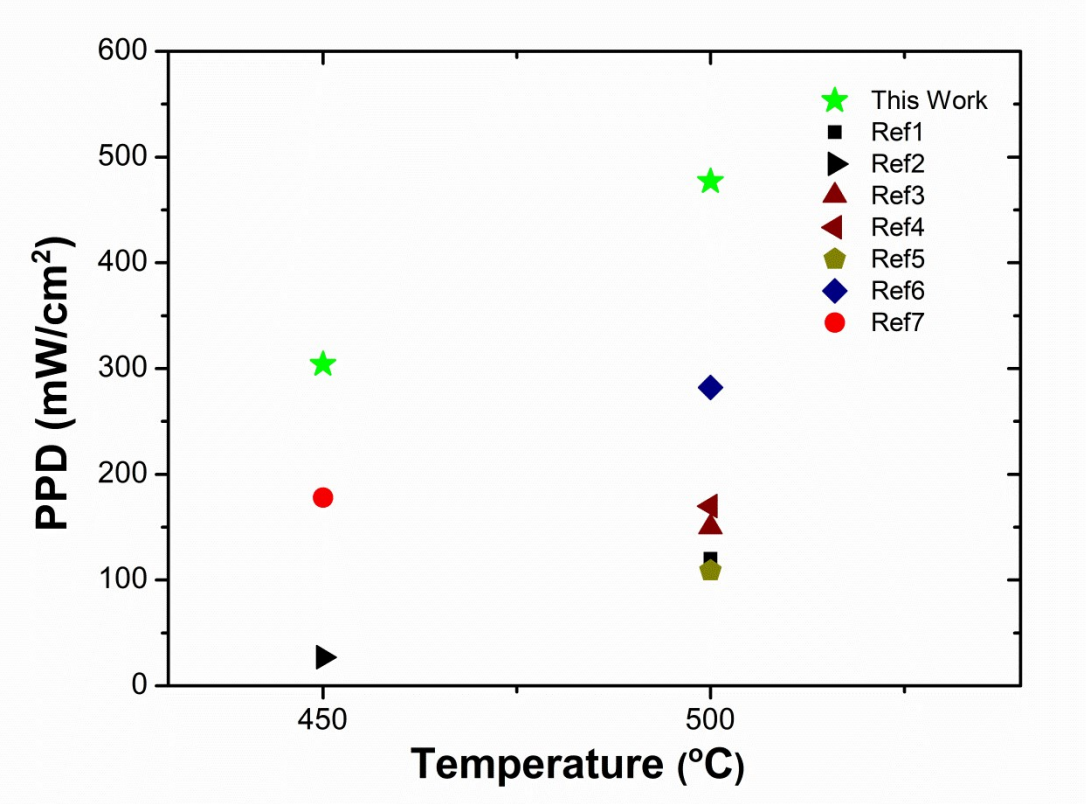

Fig. S4. Performance comparison with reported literature data related to AAO supported thin-film SOFCs. All of the references use Ni-based anode fabricated by sputtering. Hydrogen gas is used for the anode side, and the cathode is exposed to an ambient atmosphere. (PPD: peak power density)(Ref number refers to the supplementary references listed in the last section.)[1-7]

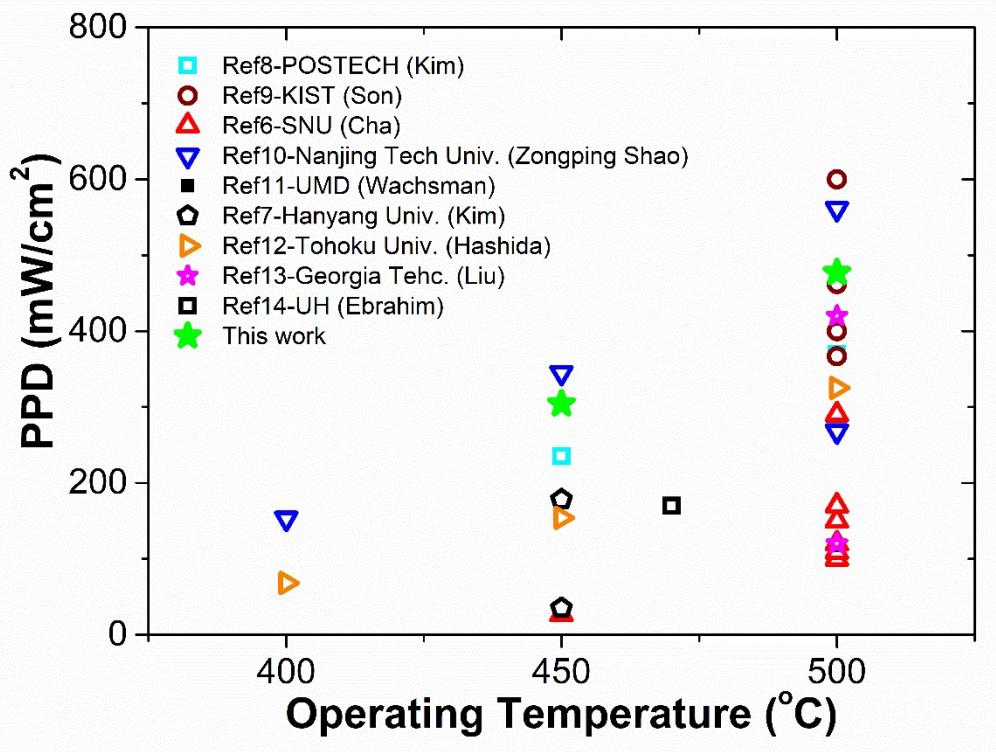

Fig. S5. Performance comparison with reported literature data related to other cell configurations.[8-14]

3. Surface FESEM analysis and image processing for TPBs length calculation.

In accordance with the model suggested by Bouvard *et al*., the average coordination number of the electronic and ionic phases can be expressed as

$$Z_{el} = 3 + \frac{Z - 3}{n_{el} + (1 - n_{el})P^2} \quad (7)$$

$$Z_{io} = 3 + \frac{(Z - 3)P^2}{n_{el} + (1 - n_{el})P^2} \quad (8)$$

$$n_{el} = \frac{\varphi_{el}P^3}{1 - \varphi_{el} + \varphi_{el}P^3} \quad (9)$$

where P ($\equiv r_{io}/r_{el}$) is the size ratio of ionic particles to electronic particles; n_{el} is the number fraction of the electronic phase; φ_{el} is the number fraction of the ionic phase; and Z is the average coordination number, typically assumed to be 6. The coordination number between electronic-phase (i) and ionic-phase (j) is given as

$$Z_{i-j} = n_j \frac{Z_i Z_j}{Z} \quad (10)$$

The probability that an i-phase particle in the percolated cluster connects the two ends of the composite;

$$P_i = \left\{1 - \left[\frac{(4.236 - Z_{i-j}}{2.472}\right]^{2.5}\right\}^{0.4} \quad (11)$$

The threshold used in this formula, introduced by Suzuki *et al*., means that Z_{i-j} value cannot be greater than 4.236.[48] The length of a neck formed between Ni and GDC particles is considered the TPB length, and neck radius is denoted as r_c.

$$r_c = \sin\theta_c \cdot min(r_{el}, r_{io}) \tag{12}$$

where θ_c is generally considered to be 15°. By combining all of these variables, the length of TPBs can be calculated as;

$$l_{tpb} = 2\pi r_c N_t n_{el} n_{io} P_{el} P_{io} \frac{Z_{el} Z_{io}}{Z} \tag{13}$$

$$N_t = \frac{1 - \varepsilon_{pore}}{\frac{4}{3}\pi r_{el}^3 \left[n_{el} + (1 - n_{el})P^3\right]} \tag{14}$$

where ε_{pore} is the volume fraction of the pore, which is measured from HR-TEM images.

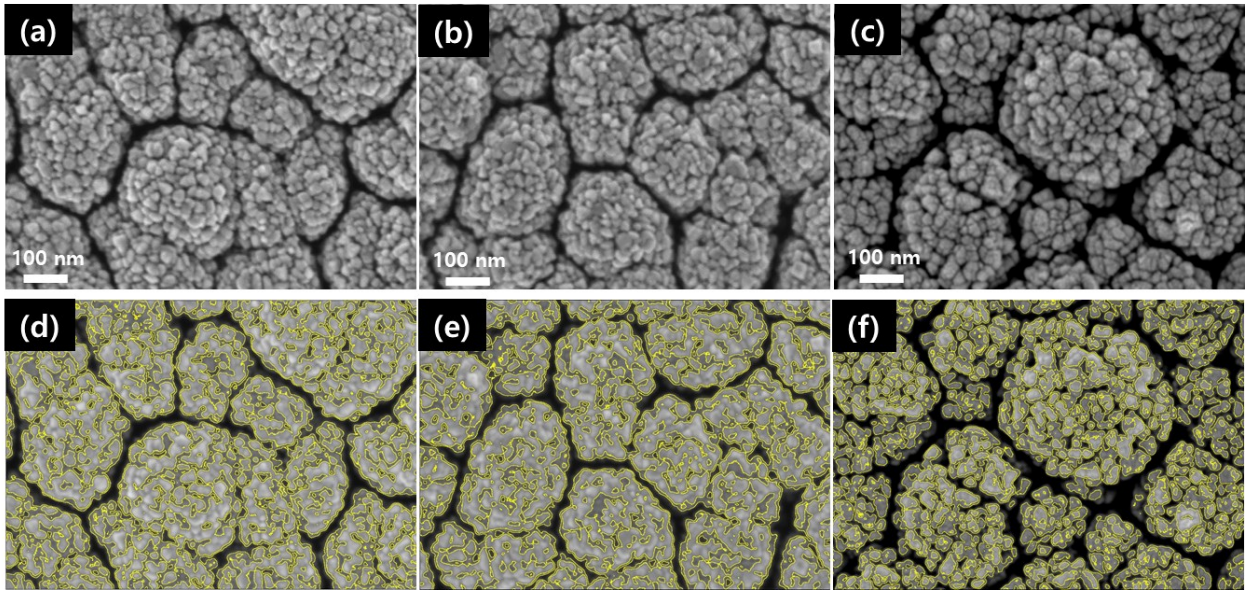

Fig. S6. Surface FESEM analysis for sputtered Ni anode varied with (a) ROT1(45°), (b) ROT2(45°), (c) ROT3(45°). Image processing for calculating TPBs length by applying volume expansion method of (d) ROT1(45°), (e) ROT2(45°), and (f) ROT3(45°). The yellow line shown in the images represents an overlapping region between Ni and pore phases that expanded to an infinitely small area.

Table S2. Comparison of TPBs density calculated by using binary-random sphere model and volume expansion method.

TPB density L_{tpb} [μm/μm^3]			
Method	ROT3(45°)	ROT2(45°)	ROT1(45°)
Binary-Random Sphere Model	66.21	84.63	91.26
Volume Expansion Method	65.26	75.83	79.08

4. Dusty gas model (DGM) applied for nanostructured anode and cathode

Mass transport equations

$$\frac{\varepsilon}{RT}\frac{\partial(y_i P)}{\partial t} = -\nabla \cdot N_i + r_i \ (mol/m^{-3}s^{-1})$$

ε:*the porosity*,N_i:*the rate of mass transport*,

r_i:*the rate of reaction inside the porous medium.*

Assumption: the diffusion process is at steady-state, and the electrochemical reactions take place at the boundary of the electrode-electrolyte interface rather than throughout the porous medium.

$$\nabla \cdot N_i = 0$$

The dusty-gas model (DGM)

$$\frac{N_i}{D_{i,k}^{eff}} + \sum_{j=1, j\neq i}^{n} \frac{X_j N_i - X_i N_j}{D_{ij}^{eff}} = -\frac{P}{RT}\frac{dX_i}{dz} - \frac{X_i}{RT}\left(1 + \frac{KP_t}{\mu D_{i,K}^{eff}}\right)\nabla P_i$$

X_i:*molar fraction*, P_i:*partial pressure*, N_i:*molar flux of gas species i.*

P_t:*total pressure*, μ *and* K :*mixture viscosity and permeability.*

$D_{i,K}^{eff}$ *and* D_{ij}^{eff} :*effective Knudsen diffusion coefficients and effective binary diffus*

Assumption: Pressure is uniform

$$\frac{N_i}{D_{i,k}^{eff}} + \sum_{j=1, j\neq i}^{n} \frac{X_j N_i - X_i N_j}{D_{ij}^{eff}} = -\frac{P}{RT}\frac{dX_i}{dz}$$

For diffusion with heterogeneous chemical reaction, the flux ratios are governed by reaction stoichiometry—Graham's law of diffusion in gaseous mixtures.

$$\sum_{i=1}^{n} N_i \sqrt{M_i}$$

M_i:*the molecular weight of component i.*

For binary component systems.

$$\frac{N_1}{D_{1,k}^{eff}}+\frac{X_2N_1-X_1N_2}{D_{12}^{eff}}=-\frac{P\ dX_1}{RT\ dz}$$

$$N_1\left(\frac{1}{D_{1,k}^{eff}}+\frac{X_2-X_1N_2/N_1}{D_{12}^{eff}}\right)=-\frac{P\ dX_1}{RT\ dz}$$

$$y_2=1-y_1, N_2/N_1=\ -\sqrt{M_1/M_2}\ (Gram's\ law)$$

$$N_1=-\frac{P}{RT}\left[\frac{1}{D_{1,k}^{eff}}+\frac{1-\alpha X_1}{D_{12}^{eff}}\right]^{-1}\frac{dX_1}{dz}$$

$$\alpha=1-\left(\frac{M_1}{M_2}\right)^{1/2}$$

$$\frac{d^2X_1}{dz^2}+\frac{\alpha}{D_{12}^{eff}}\left[\frac{1}{D_{1,k}^{eff}}+\frac{1-\alpha X_1}{D_{12}^{eff}}\right]^{-1}\left(\frac{dX_1}{dz}\right)^2=0$$

Initial conditions:

$$X_{1,\,z=0}=X_{1,bulk}$$

$$\left(\frac{dX_1}{dz}\right)_{z=0}=-\frac{JRT}{2PF}\left[\frac{1}{D_{1,k}^{eff}}+\frac{1-\alpha X_1}{D_{12}^{eff}}\right]$$

$$D_{i,K}^{eff}=D_{i,K}\frac{\varepsilon_{pore}}{\tau_{pore}}, D_{ij}^{eff}=D_{i,K}\frac{\varepsilon_{pore}}{\tau_{pore}}$$

τ_{pore}:$tortuosity\ of\ the\ pore$

$$D_{i,K}=\frac{d_p2}{2\ 3}\sqrt{\frac{8RT}{\pi M_i}}$$

d_p:$the\ mean\ pore\ diameter$

$$d_p\approx d_h=\frac{4}{(S/\varepsilon)_{pore}}$$

d_h:$the\ hydraulic\ diamter, S$:$surface\ area\ of\ the\ pore$

$$\frac{1}{D_a^{eff}}=\frac{\tau_{pore}}{\varepsilon_{pore}}\left(\frac{1}{D_{H_2-H_2O}}+\frac{1}{D_{H_2,K}}\right),\ \frac{1}{D_c^{eff}}=\frac{\tau_{pore}}{\varepsilon_{pore}}\left(\frac{1}{D_{O_2-N_2}}+\frac{1}{D_{N_2,K}}\right)$$

For the binary diffusion coefficients, Fuller-Schettler-Giddings' equation is adopted.

$$D_{ij} = \frac{0.01013T^{1.75}((1/M_i \times 10^3) + (1/M_j \times 10^3))^{1/2}}{P\left[(\sum v_i \times 10^6)^{1/3} + (\sum v_j \times 10^6)^{1/3}\right]^2}$$

$\sum v_i$: *the diffusion volume of the molecules of species i.*

The equations given above are solved by the Runge-Kutta method with Matlab.

Table S3. Geometrical Variables for 1D simulation.

Variables	*Notation*	*Value*	*Unit*
Anode grain size	d_a	3.3x10-8	[m]
Cathode grain size	d_c	2.3x10-8	[m]
Electrolyte grain size	d_e	2.2x10-8	[m]
Electrode probability	φ_{el}	0.42	
Anode tortuosity	$\tau_{pore.a}$	1.3	
Cathode tortuosity	$\tau_{pore,c}$	1.3	

References for supporting information

1 S. Ji, Y. H. Lee, T. Park, G. Y. Cho, S. Noh, Y. Lee, M. Kim, S. Ha, J. An and S. W. Cha, in *Thin Solid Films*, Elsevier, 2015, vol. 591, pp. 250–254.

2 J. Bae, I. Chang, S. Kang, S. Hong, S. W. Cha and Y. B. Kim, *J. Nanosci. Nanotechnol.*, 2014, **14**, 9294–9299.

3 S. Lee, G. Y. Cho, T. Park, Y. H. Lee, W. Yu, Y. Lee, I. Chang and S. W. Cha, *Thin Solid Films*, 2018, **666**, 177–181.

4 S. Noh, G. Y. Cho, Y. H. Lee, W. Yu, J. An and S. W. Cha, *Sci. Adv. Mater.*, 2016, **8**, 11–16.

5 Y. Kim, S. Noh, G. Y. Cho, T. Park, Y. H. Lee, W. Yu, Y. Lee, W. H. Tanveer and S. W. Cha, *Int. J. Precis. Eng. Manuf.*, 2016, **17**, 1079–1083.

6 Y. Lee, J. Park, W. Yu, W. H. Tanveer, Y. H. Lee, G. Y. Cho, T. Park, C. Zheng, W. Lee and S. W. Cha, *Energy*, 2018, **161**, 1133–1138.

7 Y. Lim, H. Lee, S. Hong and Y.-B. Kim, *J. Power Sources*, 2019, **412**, 160–169.

8 K. J. Kim, B. H. Park, S. J. Kim, Y. Lee, H. Bae and G. M. Choi, *Sci. Rep.*, 2016, **6**, 1–8.

9 H. S. Noh, K. J. Yoon, B. K. Kim, H. J. Je, H. W. Lee, J. H. Lee and J. W. Son, *J. Power Sources*, 2014, **247**, 105–111.

10 W. Zhou, Z. Shao, R. Ran, W. Jin and N. Xu, *Chem. Commun.*, 2008, 5791–5793.

11 H.-B.-R. Lee and S. F. Bent, *Chem. Mater.*, 2012, **24**, 279–286.

12 C. Ding, H. Lin, K. Sato and T. Hashida, *J. Memb. Sci.*, 2010, **350**, 1–4.

13 Y. Chen, B. deGlee, Y. Tang, Z. Wang, B. Zhao, Y. Wei, L. Zhang, S. Yoo, K. Pei, J. H. Kim, Y. Ding, P. Hu, F. F. Tao and M. Liu, *Nat. Energy*, 2018, **3**, 1042–1050.

14 R. Ebrahim, M. Yeleuov and A. Ignatiev, *Adv. Mater. Technol.*, 2017, **2**, 1700098.